Acta Geotechnica (2024) 19:7967–7988
https://doi.org/10.1007/s11440-024-02376-y

RESEARCH PAPER

Effect of stress conditions on concentrated leak erosion resistant of fine-grained soils with different characteristics

Sadettin Topçu[1] · Hasan Savaş[2] · Hasan Tosun[1,2,3]

Received: 15 January 2023 / Accepted: 8 July 2024 / Published online: 12 August 2024

Abstract

Internal erosion is one of the most important factors that cause earth structures that retain water, such as embankment dams, to collapse. Concentrated leak erosion, one of the forms of internal erosion, occurs in cracked fine-grained soils and pressurized flow conditions. To evaluate the concentrated leak erosion risk of cracks/voids, it is necessary to ascertain the erosion resistance of these materials. The erosion rate and critical shear stresses determine internal erosion resistance in concentrated leak erosion. This study determined soil's concentrated leak erosion resistance using test equipment that allowed the flow to pass through a hole with stress-free (no loading), anisotropic-compression stress, anisotropic-expansion stress, and isotropic stress conditions. The stresses that developed in the samples' hole wall where erosion occurred were determined with numerical modeling as pre-experimental stress conditions. The experiments were performed under a single hydraulic head on four selected cohesive soils with different erosion sensitivity. Time-dependent flow rates obtained from the test system can be used to determine hydraulic parameters, such as energy grade lines, with the help of basic theorems of pipe hydraulics in theoretical hydraulic models. Moreover, the erosion rates were quantitatively determined using the continuity equation, while critical shear stresses were qualitatively compared for concentrated leak erosion developed by the dispersion mechanism. As a result of the experiments, stress conditions influence the concentrated leak erosion resistance in the soil samples with dispersive erosion. Moreover, the shear strength in the Mohr–Coulomb hypothesis can explain the erosion resistance in these soils under stress conditions depending on the sand/clay ratio.

Keywords Concentrated leak erosion · Dispersive soil · Internal erosion · Swelling soil · Triaxial stress

1 Introduction

In civil engineering earthworks applications, "internal erosion" is generally defined as transporting soil particles under seepage and pressure pipe flow conditions, forming voids that further cause water transport in the media [55]. Collapse due to internal erosion is also known as seepage failure [29]. Internal erosion is considered one of the reasons why embankment dams fail [21, 53, 68]. In some developed countries where the mechanism of internal erosion in embankment dams has been studied, different terminology has been used to describe the various forms of internal erosion. According to the US bureau of reclamation (USBR) and the US army corps of engineers (USACE), the forms of internal erosion are backward erosion, concentrated leak erosion, contact erosion, global backward erosion, and suffusion/suffosion [61].

✉ Sadettin Topçu
sadettin.topcu@dpu.edu.tr

Hasan Savaş
hsavas@ogu.edu.tr

Hasan Tosun
hasantosun26@gmail.com

[1] Department of Construction Technology, Kütahya Vocational School of Technical Sciences, Kütahya Dumlupınar University, Campus of Germiyan 7.Km on Afyon Road, 43100 Kütahya, Turkey

[2] Department of Civil Engineering, Faculty of Engineering and Architecture, Eskişehir Osmangazi University, 26040 Eskişehir, Turkey

[3] Mudanya University, Bursa, Turkey

Among the forms of internal erosion considered in this study, concentrated leak erosion occurs when pressure pipe flow develops in transverse cracks and voids extending in the upstream–downstream direction of the embankment or foundations [7]. Concentrated leak erosion occurs only in cohesive soils. It is controlled by the reservoir water level above the crack/void, the length of the crack/void, and the erosion resistance of cohesive (fine-grained) soils [20]. Erosion resistance of fine-grained soils is determined by critical shear stresses (τ_{cr}) expressed as the flow velocity at which erosion starts, as well as the erosion rate ($\dot{\varepsilon}$), which indicates the rate of material transport. Fine-grained soils, also defined as dispersive soils, are highly susceptible to erosion [27]. Dispersive erosion or dispersion occurring in fine-grained soils is controlled by physicochemical repulsive forces in the clay–water system [41]. Dispersive soils can be identified using chemical approaches that consider the cations in the pore water of soils [1, 22, 30, 50]. In addition, the dispersion mechanism in fine-grained soils can be determined by various physical tests, such as the crumb test [18, 51], the double hydrometer test [16], and the pinhole test [52].

The factors involved in dispersive erosion mechanisms in fine-grained soils also affect the soil's erosion resistance. The chemical content of the eroding fluid and the pore water of fine-grained soils stand out as factors affecting erosion resistance. As the cation exchange capacity (CEC) increases, critical shear stresses increase in cohesive soils that are partially saturated [35]. In fully saturated fine-grained soils, as the pore water's sodium adsorption rate (SAR) increases, critical shear stresses decrease, and erosion rates increase [3]. Furthermore, the erosion rate decreases as the eroding fluid's total dissolved salt (TDS) increases [45]. Critical shear stress decreases at a certain SAR as pore water's TDS increases. At a given TDS of pore water, critical shear stress decreases non-linearly as SAR increases. At a certain SAR, if the water content is kept constant, critical shear stress increases as the TDS of eroding fluid increases. Similar results to those described above have also been found in consolidated fine-grained soils [47]. Critical shear stress decreases as the SAR increases in fine-grained soils that are partially saturated [2]. In addition, the temperature effect, one of the physical properties of eroding fluid, affects the erosion resistance of fine-grained soils. The erosion rate increases as the temperature of the eroding fluid increases in fully saturated fine-grained soils [6, 14]. Critical shear stresses decrease as the temperature of the eroding fluid increases in Na-Montmorillonite clay [33].

Moreover, some studies have examined the effect of geotechnical factors on erosion resistance in dispersive soils. The erosion rate in natural dispersive soils increases with increasing water content [42]. On the other hand, as dry density increases, erosion resistance increases [32, 43]. As the clay content increases in dispersive soils, erosion resistance decreases when distilled water is used as the eroding fluid [56]; in contrast, erosion resistance increases when tap water with high TDS is used as the eroding fluid [43, 65]. The effect of the degree of saturation on the erosion resistance of dispersive soils is negligible [45]. When dispersive soils are mixed with non-dispersive soils in specific proportions, the internal erosion resistance of these soils increases [40].

The erosion resistance of fine-grained soils can be determined by surface erosion tests (laboratory hydraulic flume test, pressurized flow test in closed channel, submerged-jet erosion test, and rotating cylindrical erosion test) and internal erosion tests (hole/slot or aperture erosion test and pinhole test).

The factors affecting the internal erosion resistance of fine-grained soil in embankment dams can be evaluated under material and design characteristics. In the research, plasticity index, liquid limit, clay ratio, laboratory vane shear strength, organic substance, clay mineralogy, and fine content come to the forefront as material characteristics. However, dry density, water content, compaction energy, void ratio, and degree of saturation were assessed as design characteristics.

The erosion resistance of fine-grained soils increases as the plasticity index increases [34, 35]. It decreases as the liquid limit value rises [65]. As the clay ratio increases, the critical shear stress increases while the erosion rate decreases [5, 24]. A linear relationship exists between laboratory vane shear strength and erosion resistance in fine-grained soils [17, 48]. Organic matter in fine-grained soils increases erosion resistance [36]. The erosion rate of partially saturated non-dispersive Ca-Montmorillonite clays is greater than that of dispersive Na-Montmorillonite clays [49]. Erosion resistance increases in the absence of clay minerals such as smectite and vermiculite and the presence of binding agents such as iron and aluminum oxide in fine-grained soils [65]. High critical shear stresses were observed in montmorillonite clays with high swelling potential in fine-grained soils [3]. Erosion resistance decreases as the fine content increases in the concentrated flow [65].

In fine-grained soils, the resistance to concentrated leak erosion increases as the dry density, which determines the degree of compaction, increases [5, 23, 64]. The erosion rate decreased for soils compacted on the dry side as the water content increased [4]. On the other hand, in glacial moraines, samples compacted on the dry side were eroded more than the optimum water content [25]. As the compaction energy increases on the dry side, the erosion resistance of soils increases. On the wet side, compaction energy does not affect the erosion resistance of soils [4]. In

kaolin clays, erosion resistance decreases as the compaction energy increases [12]. According to Cedeno [13], the erosion resistance of intermediate soils with high compaction energy on the wet side is higher. In partially saturated soils, critical shear stresses decrease as the void ratio increases [35]. The erosion resistance of fine-grained soils increases as the degree of saturation increases [43]. Similarly, San Lim and Khalili [46] reported that the erosion rate of unsaturated soils is higher than that of fully saturated soils.

In the studies, triaxial stress conditions that can occur on the walls of the cracks in the embankment dam are not considered factors influencing the concentrated leak erosion resistance of fine-grained soils. Therefore, this paper investigated the concentrated leak erosion behavior and erosion resistance of soil under different stress conditions using four partially saturated fine-grained soil samples with varying sensitivities of erosion. The test equipment for this study assesses stress distributions in the field by allowing flow to pass through a circular hole created in soil samples with the help of a nozzle. Soil samples were loaded stress-freely, isotropically, and anisotropically, and the stress conditions on the hole wall where erosion occurred were determined using numerical models.

2 Materials and method

The soil samples used in this study were selected to have different erosion sensitivities. Two soil samples (AF1 and AF2) were obtained from Afyon, while the other two (ÇAT and KUN) were obtained from the clay borrow fields of Çatören and Kunduzlar Dams located in Eskişehir. Physical, index, and compaction tests were performed on all soil samples. In addition, physical and chemical tests were carried out to determine the dispersibility of the soil samples, while their chemical contents and clay mineralogies were identified by XRF (X-ray fluorescence) and XRD (X-ray diffraction) analyses. Last, the erosion resistance parameters of the soil samples (i.e., critical shear stresses and erosion rates) were determined under different stress conditions using the test equipment designed for this study.

2.1 Materials

The physical, index, and compaction tests were done using the relevant standard methods [57]. The particle size distribution curves of the soil samples used in the tests are plotted in Fig. 1. Consistency limits, compaction parameters obtained using standard energy, specific gravities, and soil groups (as designated by the Unified Soil Classification System [USCS]) of the soil samples are shown in Table 1. The fine content of the soil samples is quite high. Fine contents vary between 81.1 and 62.6%. Clay ratios vary between 11.9 and 35.9%. AF1 and ÇAT samples are classified as high plasticity clay (CH), AF2 is classified as low plasticity clay (CL), and the KUN soil sample is classified as low plasticity silt (ML).

According to Table 1, soil samples were compacted at the maximum dry density and water content $w_{opt} + 2$.

The results obtained from the crumb, double hydrometer, and pinhole tests indicated that the AF1 and AF2 soil samples were dispersive. In contrast, the KUN soil sample was non-dispersive. The pinhole test results show that the ÇAT soil sample was only defined as intermediate soil (Table 2).

The chemical tests performed in the dispersivity classification are carried out using the pore water of the soils. The soil sample is saturated completely by adding distilled water at a liquid limit, and soil paste is obtained. It takes a few hours for the cations attached to the clay surfaces to dissolve completely in the pore water. Finally, soil pore water is obtained from soil paste using a vacuum filter funnel system [44]. Cation and exchange concentrations in soil pore water have been measured with an Inductively Coupled Plasma Emission Spectrometry (ICP) device to determine chemical parameters like ESP (Exchange Sodium Percentage), etc. The results of the chemical tests performed using pore water to define the dispersibility of the soil samples are shown in Table 3.

The results obtained from the chemical analysis of the soil samples' pore water were used to identify the chemical test classes of the soil samples. According to Table 4, the results of the chemical evaluation of the dispersivity of the soil samples are similar to the classifications obtained from the physical tests.

According to the XRF analysis results for the soil samples in Table 5, the Na_2O ratio in dispersive soil samples is higher than in intermediate and non-dispersive soil samples. Semi-quantitative XRD analysis was also performed on the soil samples [8]. In the AF1 and AF2 dispersive soil samples, 2:1 layered phengite belonging to the mica group [62] was identified as the dominant clay mineral, while vermiculite was identified as the dominant clay mineral in the ÇAT sample, and palygorskite was identified as the dominant clay mineral in the KUN sample (Fig. 2). In addition, as shown in Fig. 2, the XRD patterns of AF1 and AF2 dispersive soil samples are quite similar.

2.2 Test equipment

Test equipment is used for this study to investigate the concentrated leak erosion resistance of selected fine-grained soils under different stress conditions. The test equipment consisted of a water column, a loading system, and a flow-measuring system (Fig. 3).

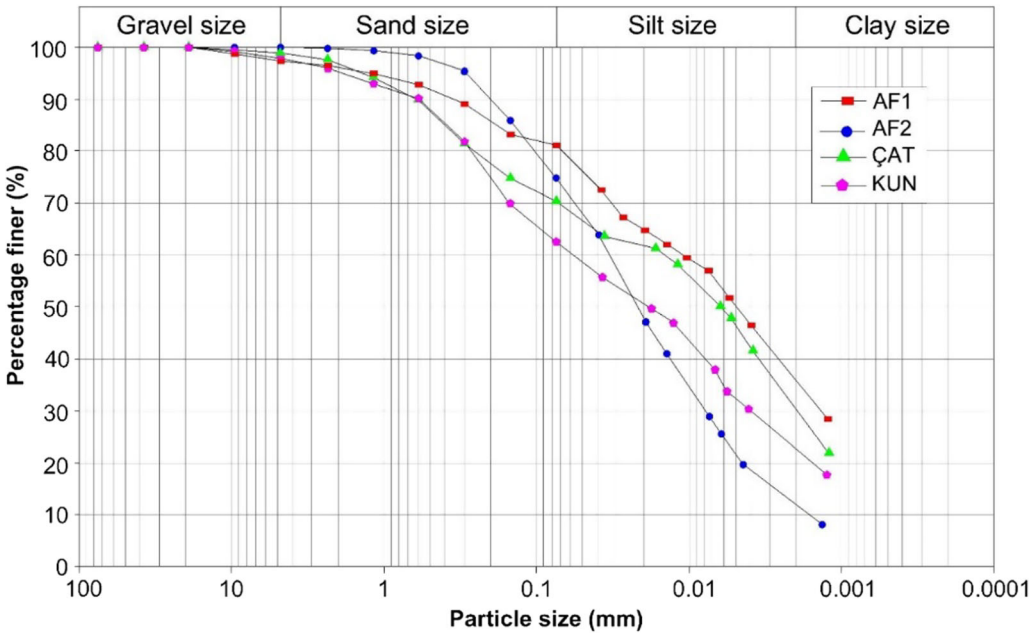

Fig. 1 Particle size distribution curves of the soil samples

Table 1 Geotechnical characteristics of soil samples

Sample	Consistency limits (%)			Compaction parameters		Gs	Group
	LL	PL	PI	ρ_{dmaks} (Mg/m^3)	w_{opt} (%)		
AF1	59	29	30	1.535	22.3	2.68	CH
AF2	43	26	17	1.508	20.1	2.65	CL
ÇAT	53	28	25	1.70	18.0	2.75	CH
KUN	48	28	20	1.54	21.5	2.69	ML

Table 2 Physical test results

Sample	Crumble test[a]	Double hydrometer test[b]	Pinhole test[c]
AF1	G3	D-77.5%	D1
AF2	G3	D- 69.0%	D1
ÇAT	G1	ND- 0%	ND3
KUN	G1	ND- 0%	ND1

a According to the [58], G1: Non-dispersive, G2: Intermediate, G3, G4: Dispersive. *b* According to the [59], % Dispersion < 30: Non-dispersive (ND), 30–50: Intermediate (I) > 50: Dispersive (D). *c* According to the [60], ND1, ND2: Non-dispersive, ND3, ND4: Intermediate, D1, D2: Dispersive

Table 3 Chemical test results

Sample	EC (mmhos/cm)	pH	TDS (meq/L)	Na (%)	SAR	ESP (%)	CEC (meq/100 g)
AF1	14.93	9.3	112.9	79.5	22.72	30.23	21.37
AF2	20.2	9.67	152.21	98.26	131.17	52.35	23.46
ÇAT	1.151	8.33	10.41	46.69	2.96	6.29	19.12
KUN	0.427	8.27	4.65	12.9	0.42	0.68	17.38

Table 4 Chemical test classes

Sample	TDS-Na (%) [50]	CEC-ESP (%) [22]	ESP (%) [1]
AF1	A-Dispersive	HD-High dispersive	D-Dispersive
AF2	A-Dispersive	HD-High dispersive	D-Dispersive
ÇAT	C-Intermediate	MD-Moderate dispersive	ND-Non-dispersive
KUN	B-Non-dispersive	ND-Non-dispersive	ND-Non-dispersive

The water level was kept constant during the experiment due to the cylindrical overflow vessel in the water column system. A submersible pump transferred water from the feeding chamber to the cylindrical overflow vessel. A loading system was developed to experiment with soil samples under desired stress conditions. The longitudinal section of the modified stress control triaxial equipment (MSCTE) is shown in Fig. 4.

With the MSCTE, axial tensile and compressive stresses were applied to soil samples in addition to ambient

Table 5 XRF analysis results for the soil samples

Sample	SiO_2	Al_2O_3	Fe_2O_3	MgO	CaO	K_2O	TiO_2	MnO	P_2O_5	Cr_2O	NiO	Na_2O	SO_3	Cl	IL
AF1	52.14	16.58	6.47	1.68	5.13	3.42	0.69	0.15	0.11	–	0.04	1.61	0.13	0.1	11.75
AF2	59.16	16.89	5.76	1.57	1.51	3.97	0.68	0.12	0.11	–	–	2.6	0.29	0.16	7.19
ÇAT	41.02	11.32	9.22	9.22	8.54	2.53	0.86	0.24	0.17	0.1	0.1	0.9	0.6	–	16.53
KUN	32.69	7.25	6.04	5.29	21.98	1.17	0.6	0.19	0.07	0.09	0.08	0.22	0.05	–	24.30

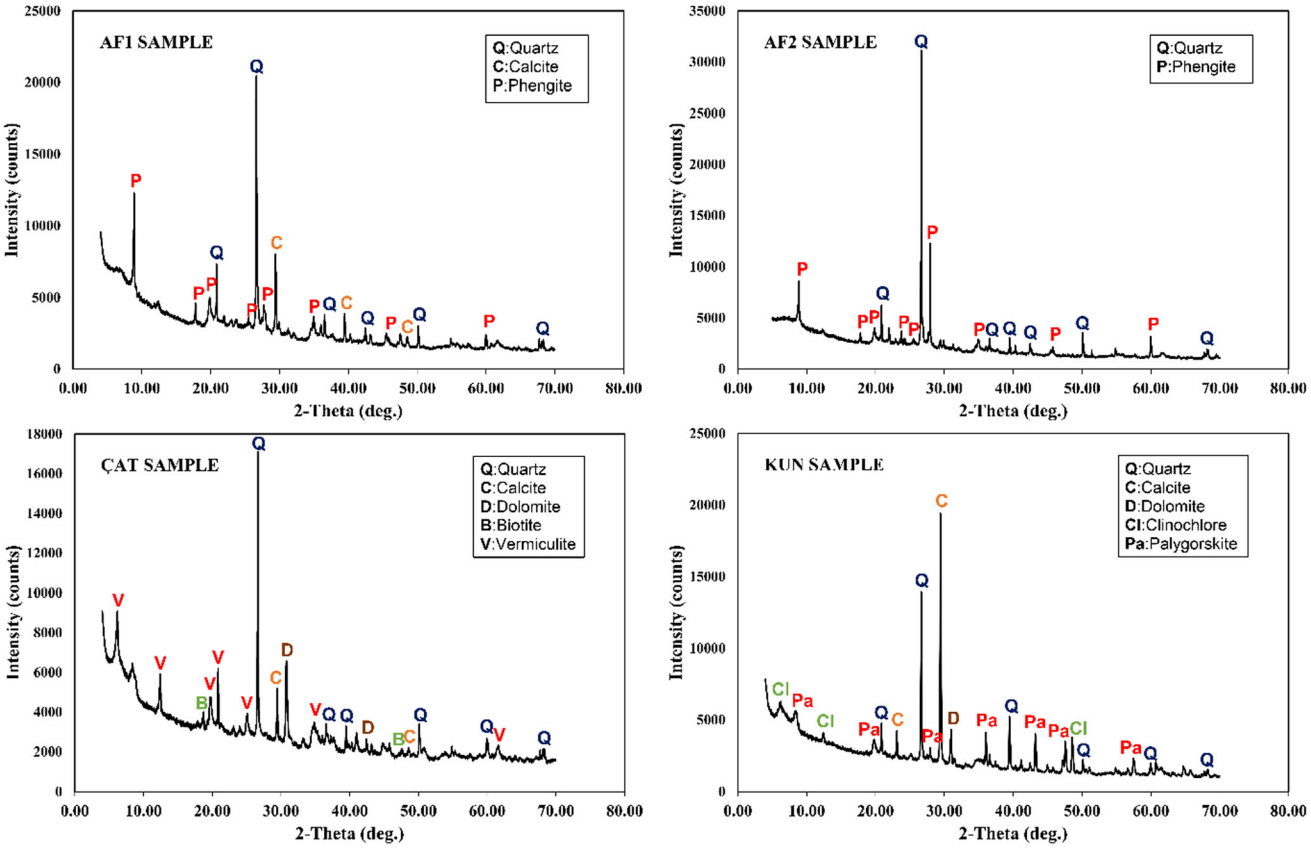

Fig. 2 Curve of XRD results of soil samples

pressure. The load was transferred to the sample by amplifying it at 1:5 on the tensile arm and 1:10 on the compressive arm through tensile and compressive loading frames. Calibration was performed in the equipment for compressive stresses between 50 and 300 kPa and tensile stresses between 25 and 150 kPa. The cell was stabilized during the test by being attached to the bottom plate with two lever clamps. The cell was a triaxial test cell. Unlike the triaxial test cell, entrance and exit isolating valves were attached to the bottom plate of the cell to allow flow to pass through the hole. In addition, a feed/discharge valve was used during the experiments to fill and discharge the water in the cell. Flow was provided to the hole in the soil sample with the help of a nozzle. A wire-mesh strainer with an aperture size of 2 mm was placed on the base adapter where the sample was put. The material transport in the soil samples prepared by sieving through a No.10 sieve was ensured to take place easily with this wire-mesh strainer. In the soil sample, the ambient pressure was created by an oil/water constant pressure unit with a capacity of 1700 kPa, and it was monitored on a screen via a pressure transmitter connected to a data logger. Axial deformations in the soil sample were measured with a displacement transducer. The piston was combined with the upper adapter by a locking apparatus. A slot on the locking apparatus allowed the piston to move in one direction. An interlocking system was achieved inside the edge of the piston and slot. It was

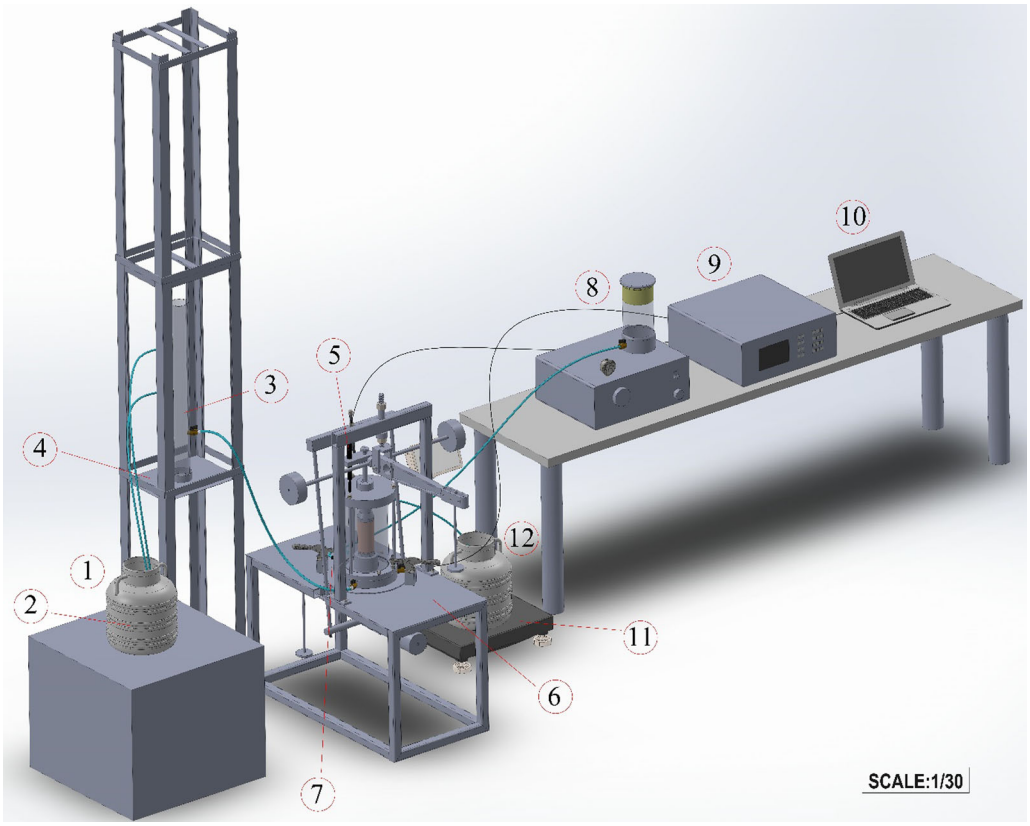

Fig. 3 Test equipment: **Water Column System**: 1. Feeding chamber; 2. Submersible pump; 3. Overflow vessel; 4. Height-adjustable platform. **The Loading System**: 5. Displacement transducer; 6. MSCTE; 7. Pressure transmitter; 8. Oil/water constant pressure unit; 9. Data logger; 10. Monitor. **Flow-Measuring System**: 11. Balance; 12. Collection chamber

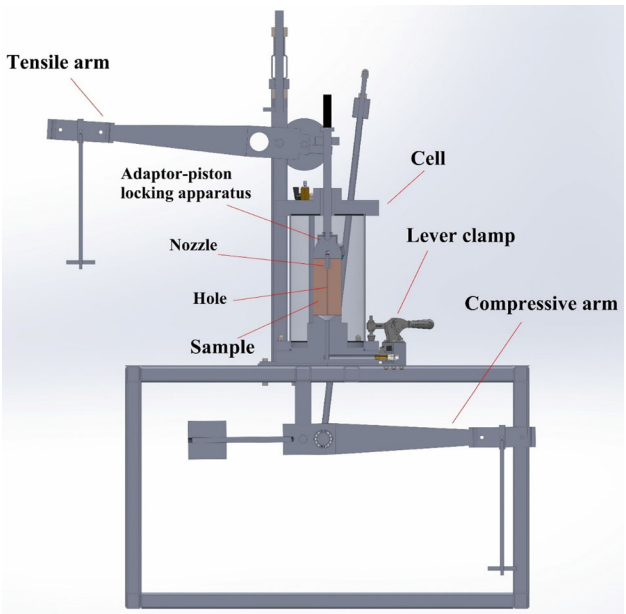

Fig. 4 Longitudinal section of MSCTE

locked when the piston entering this slot was rotated 90° in any direction.

The flow rate passing through the hole created in the soil sample was measured with a flow-measuring system that consisted of a digital scale and a collection chamber. The volume values were obtained by dividing time-dependent weight data by the density of water at the measured temperature. Flow rates were also calculated from time-dependent volume values.

2.3 Determination of hydraulic model and capacity

The basic principles of pipe hydraulics were used to determine the hydraulic parameters, such as the energy grade line (i) of the flow through the hole created in the soil sample. In pipe hydraulics, flow is considered fully developed and uniform. For this study, it was ensured that the flow could be fully developed and uniform, especially passing from the overflow vessel to the plastic pipe and from the nozzle to the hole.

In the test equipment, experiments were carried out under a single hydraulic load. Equation (1) obtained from the Bernoulli equation was used to determine the energy of

the hydraulic models in the test equipment. The height difference between the overflow vessel's water surface and the outlet pipe's end is 1.09 m. Two points were considered while adjusting that height difference. The first was that the pipe axis elevation coming out of the overflow vessel was higher than the initial elevation of the hole to prevent air formation in the sample due to low-pressure heads. (The solubility of gases dissolved in water decreases as pressure decreases.) The second point was to avoid excessive turbulence in the hole in the sample, which occurs in turbulent flows and causes errors in calculating major head losses.

$$1.09 = \frac{V_{ex}^2}{2g} + \Sigma\Delta h \quad (1)$$

V_{ex}: average velocity of the flow exiting the pipe, $\Sigma\Delta h$: total head loss (the sum of major and minor head losses), g: gravitational acceleration.

To determine the hydraulic capacity of the test equipment, aluminum molds with the same dimensions as the soil samples but different hole diameters (1, 2, 3, 4, 6, 8, 10, 12, and 14 mm) were used. The flow rates were obtained by passing water flow for each hole diameter at the hydraulic load specified in Eq. (1). In the physical model, the increase in flow rate between 1- and 4-mm hole diameters was linear with $R^2 = 0.9951$. Therefore, the time-dependent flow rate increase between the initial (first) hole diameter ($d_i = 2$ mm) and the final (last) one ($d_f = 4$ mm) was considered to be linear based on the continuity equation in calculating the erosion rate in eroded soil samples. Major (the head losses in pipes due to viscous effects) and minor (the head losses caused by changes in the direction and magnitude of the flow velocity in pipe components) head losses were determined in the test equipment. Flow rates obtained in the physical model considering head losses were used to calculate the sum of major and minor head losses ($\Sigma\Delta h$) in the SF Pressure Drop 7.2 program for hole diameters of 2, 3, and 4 mm, and then theoretical hydraulic models were created. Cock and isolating valves with a hole diameter of 2 mm were not taken into account in calculating head losses because the flow was laminar. In addition, there was no head loss in the wire-mesh strainer with a 2-mm aperture of the same hole diameter. In calculating major head losses, for $R_e < 3000$, the flow regime was accepted as laminar, while for $R_e > 3000$, it was considered to be turbulent. Friction coefficient values were obtained from the Moody diagram under laminar and turbulent flow conditions. The Darcy–Weisbach equation was used to calculate major (friction) head losses. Hydraulic roughness (k_s) on the walls of the holes in plastic and aluminum pipes in the test system was accepted to be 0 mm, based on the theoretical study by Yunus [66]. Because the viscous sublayer was higher than

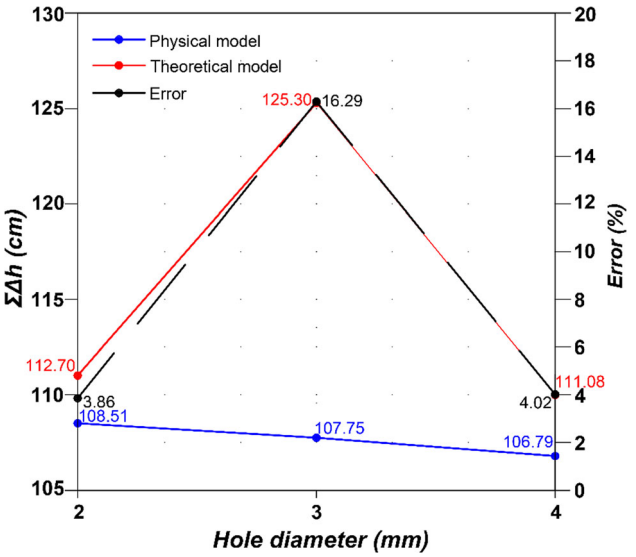

Fig. 5 Total head losses in physical and theoretical hydraulic models

k_s due to low flow rates, the smooth-pipe value ($k_s = 0$ mm) was accepted for the hole walls of the aluminum molds [67]. The total head losses in the theoretical hydraulic models created by using aluminum sample molds and in the physical hydraulic model obtained (Fig. 5).

The error in the 3-mm hole diameter between the physical and theoretical hydraulic model is higher than those in the other two diameters because the flow regimes in the plastic and aluminum pipes were in the critical region, according to the Moody diagram. The friction coefficient values in the critical region are uncertain. The reason for the slight difference between the head losses for hole diameters of 2 and 4 mm is that, as pipe diameters decrease, the similarity between theoretical and physical models decreases in conventional methods, such as with the Moody diagram [28].

2.4 Determination of stress conditions with numerical modeling

In conventional triaxial test systems, axial and radial stresses act on cylindrical soil samples. For the soil samples used in this study, different stress conditions occurred that were unlike those found in conventional systems due to the nozzle slot and hole through which the flow was passed. The stresses formed in hollow cylindrical parts due to ambient pressure and axial loading include axial, tangential, and radial stresses [11]. Accordingly, the loads that acted on this study's soil samples and the stresses formed in the soil samples (Fig. 6). The axial stresses acting on the soil samples' flow direction (σ_1) also act on its hole wall (σ_a).

Tangential and radial stresses form in hollow cylindrical parts due to ambient pressure, while axial stresses develop due to loads applied in the axial direction of hollow

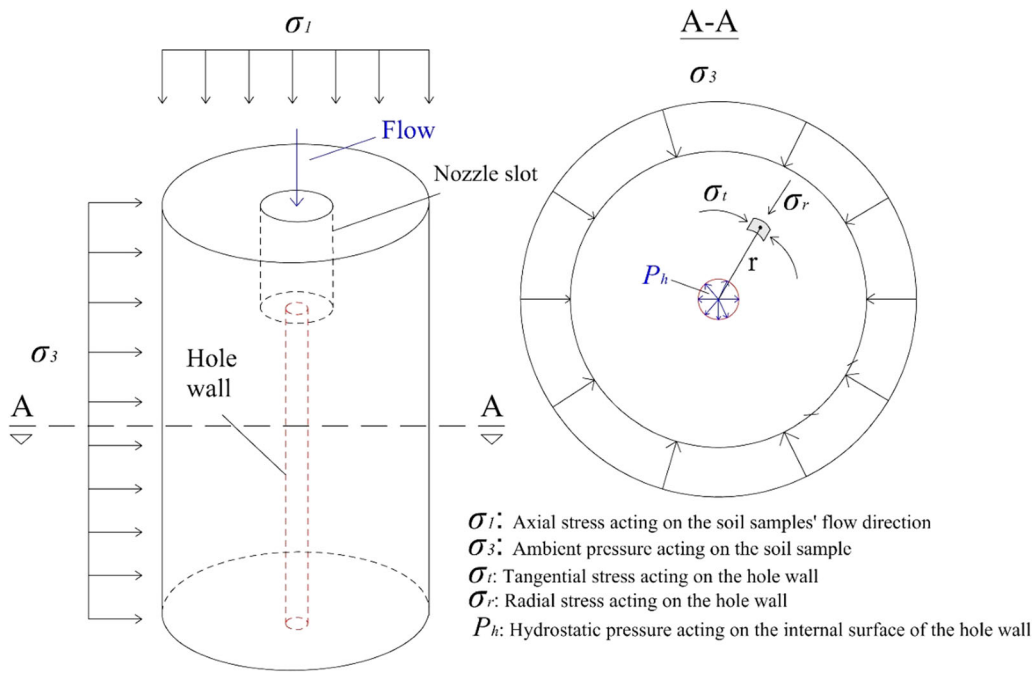

Fig. 6 Stresses acting on the soil samples' hole wall

cylindrical parts. Due to the flow in the soil sample, hydrostatic pressure is generated in the hole wall. In experimental studies, hydrostatic pressure in the hole wall is very low compared to the tangential, radial, and axial stresses acting on the hole wall. Therefore, it was considered negligible, and $P_h = 0$ was assumed. If the flow through the crack was to occur in the body or foundation of a real embankment dam, the hydrostatic pressures acting on the crack walls could be larger depending on the reservoir water height and, therefore, need to be considered together with the stresses in situ. Especially in dispersive soils where erosion occurs, stress conditions on hole walls are typically regarded as pre-experimental (pre-erosion developed by flow) stress conditions due to the sudden and rapid development of the erosion and the slight change in hole diameters widened by erosion. The numerical model realized is also only a mechanical model. Moreover, the soil samples are partially saturated. Therefore, the deformations are not due to consolidation (deformation due to the decrease of excess pore water pressure). The deformations here are due to reduced air volumes in the soil samples. For this reason, the stresses developed along the hole wall in samples kept under stress conditions for 24 h are evaluated based on total stresses.

The workbench module of ANSYS v.14 software was used to determine the stresses on the hole wall, which was considered where erosion formed. The stresses developed in the hole wall were determined numerically by modeling in three dimensions with the finite element method. The boundary conditions of the nozzle slot were defined by the cylindrical support where radial deformations were limited. The movement of the contact surfaces between the nozzle and the soil sample was restricted in the tangential and normal directions. The base surface of the sample where the flow exited the hole was confined to prohibit displacements and rotations in all directions. In the experiments carried out under triaxial stress conditions, the geometric model, created with numerical modeling to determine the stresses developing on the hole wall, consisted of 130,763 nodes and 94,051 tetrahedron elements (Fig. 7). The mean skewness criterion of the elements in the geometric model was 0.239, and, according to [39], this

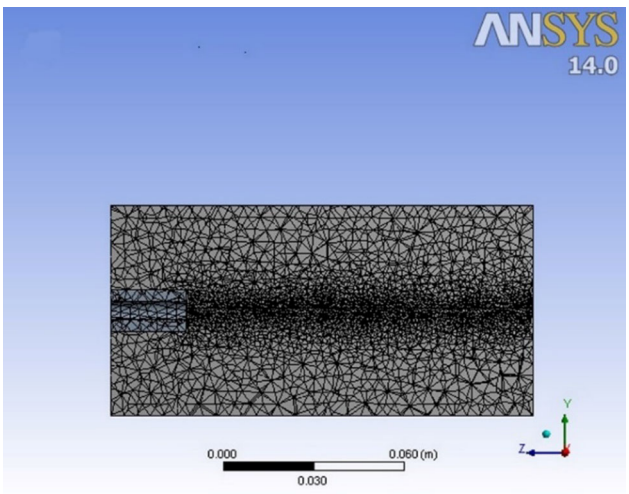

Fig. 7 Longitudinal section of the geometrical model

means that it was a perfect (excellent) geometric model because the value was between 0 and 0.25.

Because very small axial deformations were obtained due to loading conditions during the experiments, it was assumed that the soils showed linear elastic material behavior in the numerical modeling. In addition, it was accepted that the soils were isotropic homogeneous materials. Experimental studies were performed on the soil samples under four loading conditions (Table 6). While ambient pressures were kept constant, axial stresses were changed, and samples were loaded. In other words, under anisotropic loading conditions, the confining pressures, $\sigma_1 = \sigma_3 = 100$ kPa, were applied, and then the axial stress, $\sigma 1$, was changed. Thus, this study's experiments were carried out under isotropic and anisotropic loading conditions.

In this study, axial strains measured during the tests were used to see the degree of calibration of the numerical modeling. Axial deformations (ΔL) were measured in the samples under the loading conditions above, and axial strains were calculated as $\varepsilon_a = \Delta L/L_o$, where L_o was the initial length of soil samples. The elastic modulus values used in this study's numerical modeling were obtained using the axial strains measured during the experiments. The parameters that determine the stress–strain behavior of the soil in the linear elastic material model are elastic modulus (E) and Poisson's ratio (v). Briaud [10] states that the elastic modulus, under triaxial stress conditions, is not equal to the slope of the stress–strain curve; furthermore, different elastic modulus values and Poisson ratios can be obtained under various stress conditions. Therefore, for anisotropic loading conditions, the elastic modulus values of soil samples were calculated by using the axial strains obtained for isotropic loading conditions (ε_{ai}), according to Eq. (2) stated in Farzin et al. [19].

$$E = \frac{\sigma_1 - \sigma_3}{\varepsilon_a - \varepsilon_{ai}} \tag{2}$$

Equation (3) was used to calculate elastic modulus values under isotropic loading conditions [10]. According to Oh and Vanapalli [38], depending on the saturation degree of soil samples, the Poisson ratio (v) was taken as 0.47 for anisotropic loading conditions, while it was taken as 0 for isotropic loading conditions because the radial strain is equal to the axial strain and the cylindrical cross-sectional area of samples does not change. The values of the elastic modulus for each soil sample at different loading conditions are given in Table 7.

$$E = \frac{\sigma_1 - 2v\sigma_3}{\varepsilon_a} \tag{3}$$

When the axial deformations obtained from the numerical modeling and the experimental studies are compared, it can be seen that the numerical modeling yielded results very similar to the measured ones (Fig. 8).

In numerical modeling, the normal stresses on the hole wall vary along the hole length. Therefore, the arithmetic mean of these stresses was considered. The principal stresses (σ_{1h}, σ_{2h}, σ_{3h}) along the hole wall, as determined by the numerical modeling for three different loading conditions and with hole diameters of 2, 3, and 4 mm.

For the hole with a diameter of 2 and 3 mm, the maximum principal stresses are tangential stresses, while the minimum principal stresses are radial stresses under all loading conditions. For the hole with a diameter of 4 mm, the maximum principal stresses are the axial stresses only in loading no. 4, while the minimum principal stresses for this diameter under all loading conditions are the radial stresses. The average principal stress ratios (σ_{1h}/σ_{2h}, σ_{2h}/σ_{3h}, and σ_{1h}/σ_{3h}) calculated for each hole increased due to erosion (Table 8).

Radial stresses determine the change of the initial hole diameter ($d = 2$ mm) formed while preparing soil samples under the given loading conditions. In the analyses made by considering the lowest elastic modulus value for the soil samples under three different loading conditions, it was observed that the initial hole diameter showed negligible deformation.

2.5 Evaluation of the data

Flow rates increased in soil samples where erosion occurred, while in soil samples with a constant hole diameter and

Table 6 Loading conditions applied to the soil samples

Loading no	Loading conditions			Loading type
	σ_1 (kPa)	σ_3 (kPa)	K_d*	
1	0	0	–	Stress-free condition
2	66.7	100	1.5	Anisotropic-expansion
3	100	100	1	Isotropic
4	150	100	0.67	Anisotropic-compression

*$K_d = \sigma_3/\sigma_1$

Table 7 Elasticity modulus used in numerical modeling

Loading no	Elasticity modulus, E, kPa			
	AF1	AF2	ÇAT	KUN
2	10,122	17,254	9514	8495
3	20,896	13,333	18,421	14,894
4	12,500	13,514	15,576	16,234

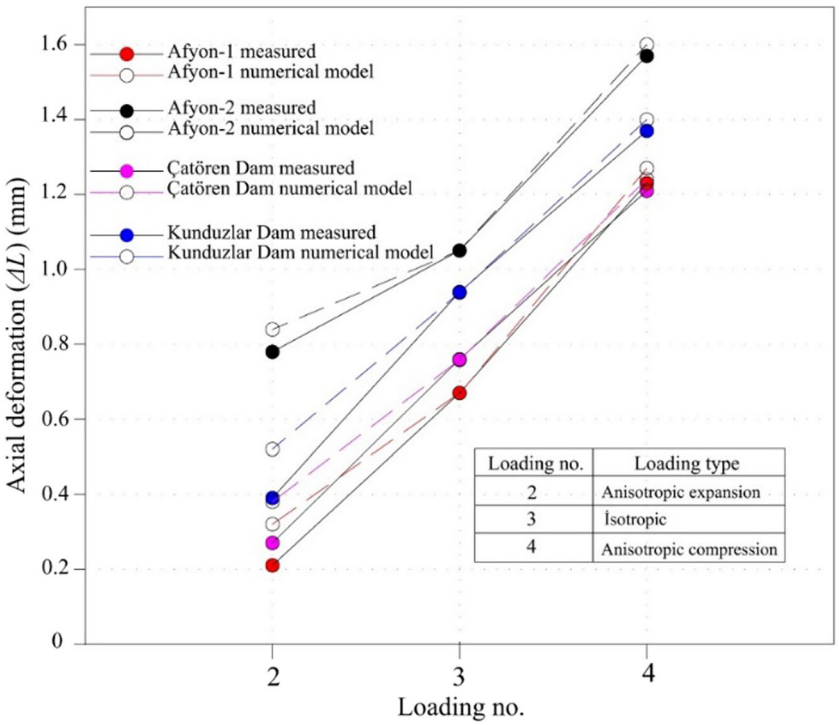

Fig. 8 Axial deformations measured during the experiments and numerical modeling

Table 8 Average principal stress ratios on the hole wall

Loading no	σ_{1h}/σ_{2h}	σ_{2h}/σ_{3h}	σ_{1h}/σ_{3h}
2	2.11	1.44	3.10
3	1.59	2.08	3.42
4	1.14	2.61	2.96

no erosion, flow rates did not change over time, or they changed negligibly. Moreover, flow rates went toward zero in the samples where erosion did not occur, but the hole diameter decreased over time. In examples where the hole diameter decreased over time, the recovery time of the hole (t_{recovery}) and the cumulative water volume passing through the hole during the measurement period (ΣV) were considered. Only the cumulative water volume was evaluated during the measurement period in the samples where the hole did not expand but remained constant.

The procedure below was followed to evaluate the data on the eroded soil samples:

1) The time-dependent flow rate curve was drawn from the experiments. In the time-dependent curve, Q_2 (the flow rate obtained at the initial hole diameter [d_i] of 2 mm) and t_2 or t_i (the time erosion starts) were determined. However, flow rates less than 15.63 mL/s (the flow rate obtained for $d_f = 4$ mm in the physical hydraulic model) were considered when determining t_4 or t_f, the time erosion ends. Among these low flow rates, the point that gives the highest regression coefficient of linearity was identified as Q_4, the flow rate at the end of erosion. A time-dependent flow curve was drawn for the distance between these two determined points, which would be used in calculating the erosion rate (Fig. 9).
2) A time-dependent curve of the hole diameter was drawn based on the time the erosion started and ended (the initial hole diameter was 2 mm, while the final hole diameter was 4 mm) (Fig. 10). The equation of the line, $d = mt + 2$, was determined, and the time that the hole diameter was 3 mm (t_3) was determined from this equation.
3) By using $Q = at + b$, which is the equation of the line in the time-dependent flow rate curve used to calculate the erosion rate (see Fig. 9), the flow rate when the hole diameter was 3 mm (Q_3) could be calculated for t_3.
4) In this study, it was accepted that the hole, which was first formed circularly, would enlarge due to erosion. So, erosion rate ($\dot{\varepsilon}$) was calculated as $\dot{\varepsilon} = \frac{\rho_d}{2}\frac{\Delta d}{\Delta t}$ where ρ_d is dry density [65].
5) For each soil sample, by using Q_2, Q_3, and Q_4 flow rates in the theoretical hydraulic models created for hole diameters of 2, 3, and 4 mm, the hydraulic roughness on the hole surface (k_s) and the energy

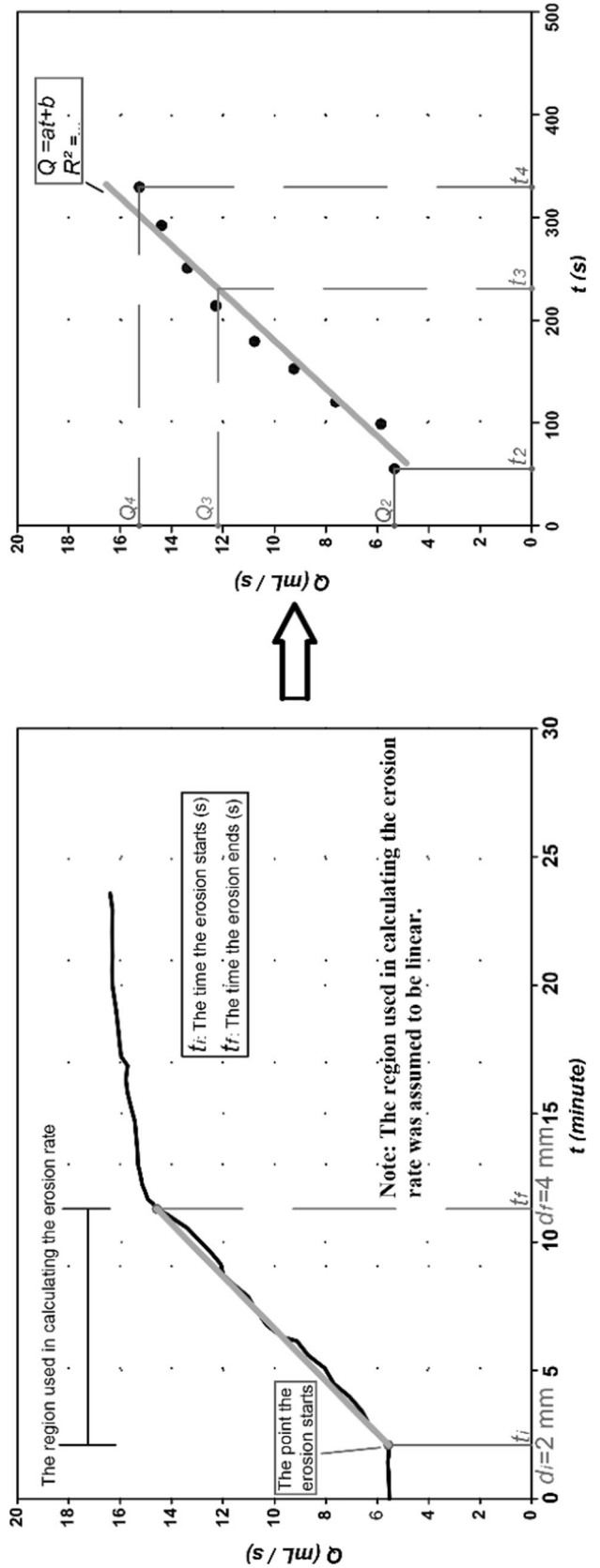

Fig. 9 Flow rate-time graph considered in the erosion rate calculation

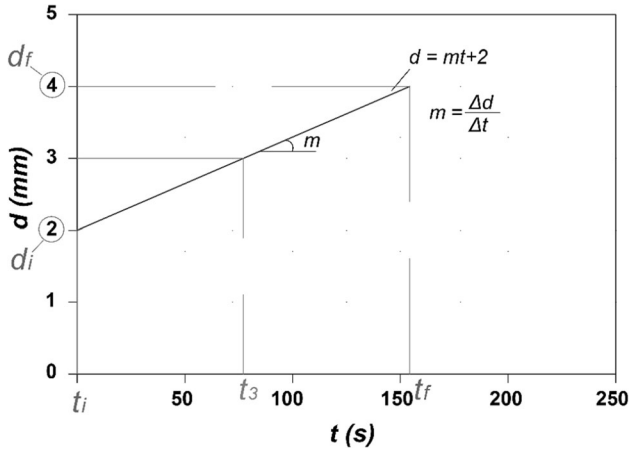

Fig. 10 Change in hole diameter with time

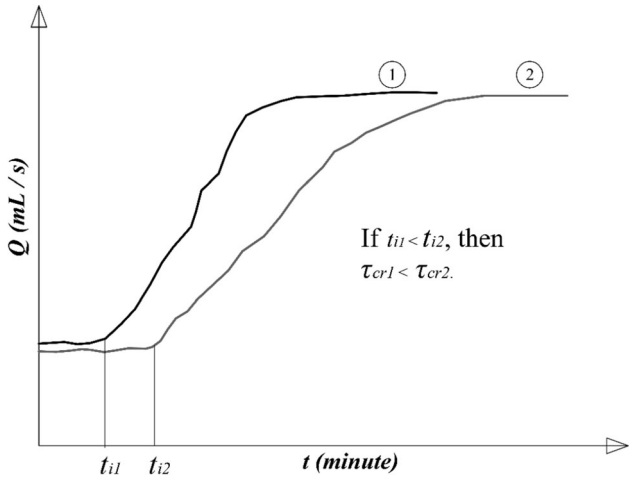

Fig. 11 Comparison of critical shear stresses for soil samples

gradient of the experiments (i) were determined according to the total head loss ($\Sigma\Delta h$) calculated from the Bernoulli equation (see Eq. 1). Depending on the hole surface's hydraulic roughness, the energy gradient was calculated by dividing the friction head loss ($\Delta h_{friction}$) by the hole length.

6) Critical shear stresses (τ_{cr}) were qualitatively compared by considering the time when erosion began (t_2). As t_2 increased, critical shear stresses increased (Fig. 11).

On the other hand, the energy gradient was calculated using the theoretical hydraulic model for Q_2 values for the soil samples that were not eroded. Raw flow rates were smoothed in these soil samples with the negative exponential method. In addition, Reynolds numbers, Re, were calculated using the flow rates obtained from the hole diameters in each sample. Further details about the process used to evaluate the data can be found in [56].

At the beginning of the experiment, the target compaction characteristics were checked. The error between the target and measured water contents, $\Delta(\%)$, was determined. The saturation degree of the soil samples (S_r) was calculated. The density of water at room temperature (20 °C) was used. Volumetric changes in loading conditions were neglected, and S_r was calculated by using the wet density value (ρ_{wet}), target dry densities ($\rho_{d\max}$), and water content measured at the end of the experiment (w).

Soil samples were coded for convenience in presenting the findings of the experimental study. An example is shown below:

Sample abbreviation_ loading number, experimental method: AF1_3WL.

- Sample abbreviation: Afyon-1: AF1; Afyon-2: AF2; Çatören Dam: ÇAT; Kunduzlar Dam: KUN.
- Loading number: 1, 2, 3, 4 (see Table 6).
- Experimental method: WL: performed under the given loading condition by waiting 24 h; C: performed on the samples kept in a curing environment for 24 h without loading; IL: performed immediately under the given loading condition.

2.6 Experiments

A flow chart (see Fig. 12) summarizes the experiments performed and describes the step-by-step evaluation process for the data. Distilled water was used as the mixing water while preparing soil samples. The soil mixed with distilled water was then compacted with a system consisting of a mold, rammer, and needle manufactured from brass (Fig. 13). Soil samples were compacted in seven layers. The compaction thickness was decreased toward the upper layers to achieve the same degree of compaction throughout the soil sample. The compaction was achieved by keeping the percentage by weight in each layer the same (14%), except for the nozzle area (16%), thus preventing over-compaction of the lower layers while the upper layers were compacted. Each layer is pinned so that the layers fit together well. Each soil sample removed from the mold was checked for joints between the layers. The needle used to create holes in the soil samples adheres to the soil with the effect of water, making it impossible to pull it out by hand. The needle must first be carefully loosened by tapping the end of the needle with a plastic mallet and then slowly pulled out by holding the needle's cap under the mold. The soil sample used in the experiments was 70 mm in diameter and 140 mm in height. The hole length through which the flow passed was 115 mm.

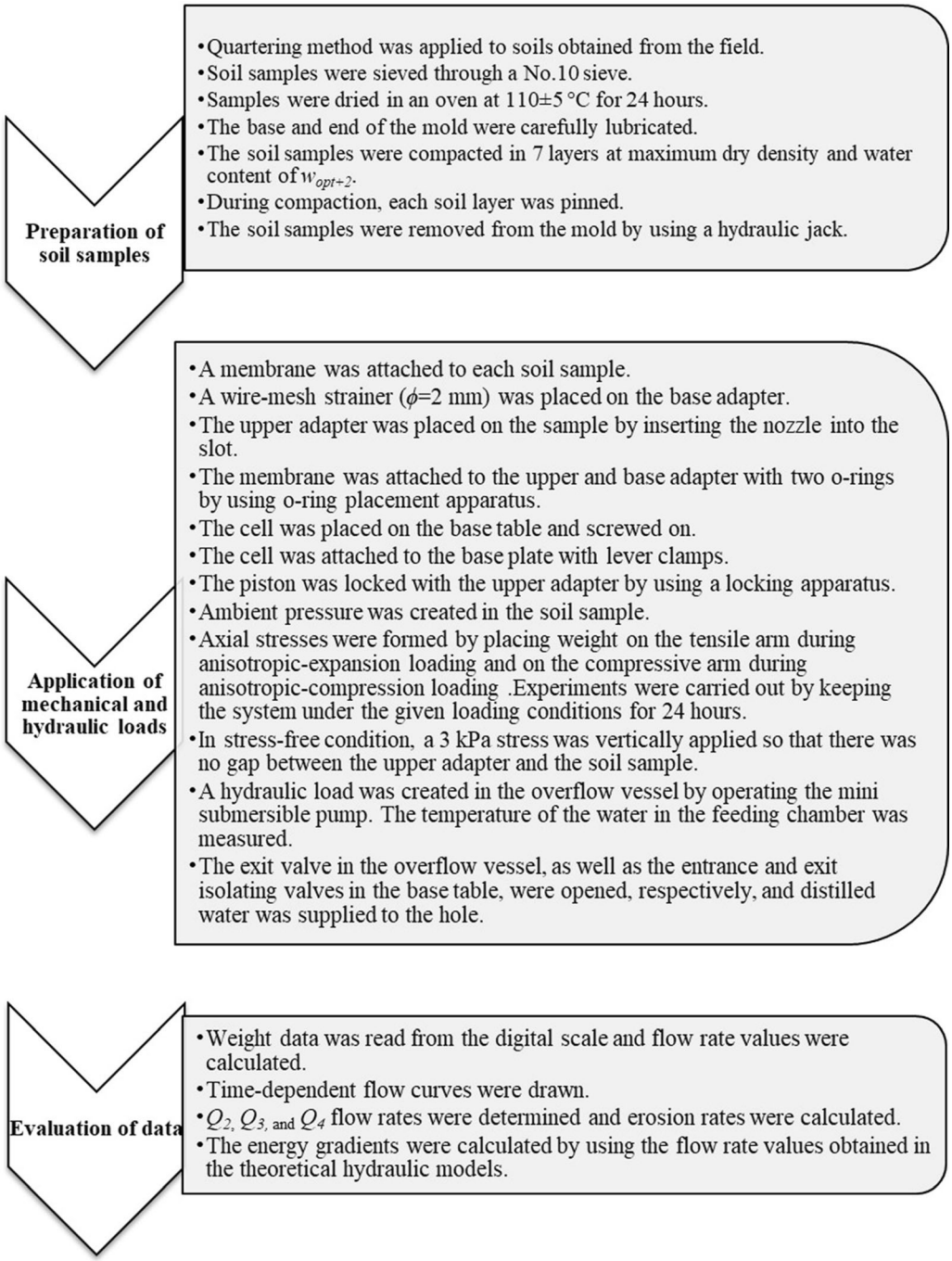

Fig. 12 Flow chart of the experimental procedure

3 Results and discussion

The measured and target water content values obtained at the end of the experiments and the saturation degrees of the samples are shown in Table 9. As stated in Table 9, except for the AF2 soil sample, water content values were very close to the target values. In addition, the soil samples were almost equivalent in terms of physical properties under different loading conditions.

The time-dependent flow rate curves of AF1 and AF2 dispersive soil samples were given under different loading conditions in Figs. 14 and 15, respectively. The erosion process develops and ends very fast (5–10 min). Again, the water flow is given only to the hole with the help of a nozzle. Therefore, a very small and limited area around the eroded hole becomes fully saturated. This is almost negligible. This saturation is certainly not observed in the whole soil sample. Dispersive erosion occurred in the hole

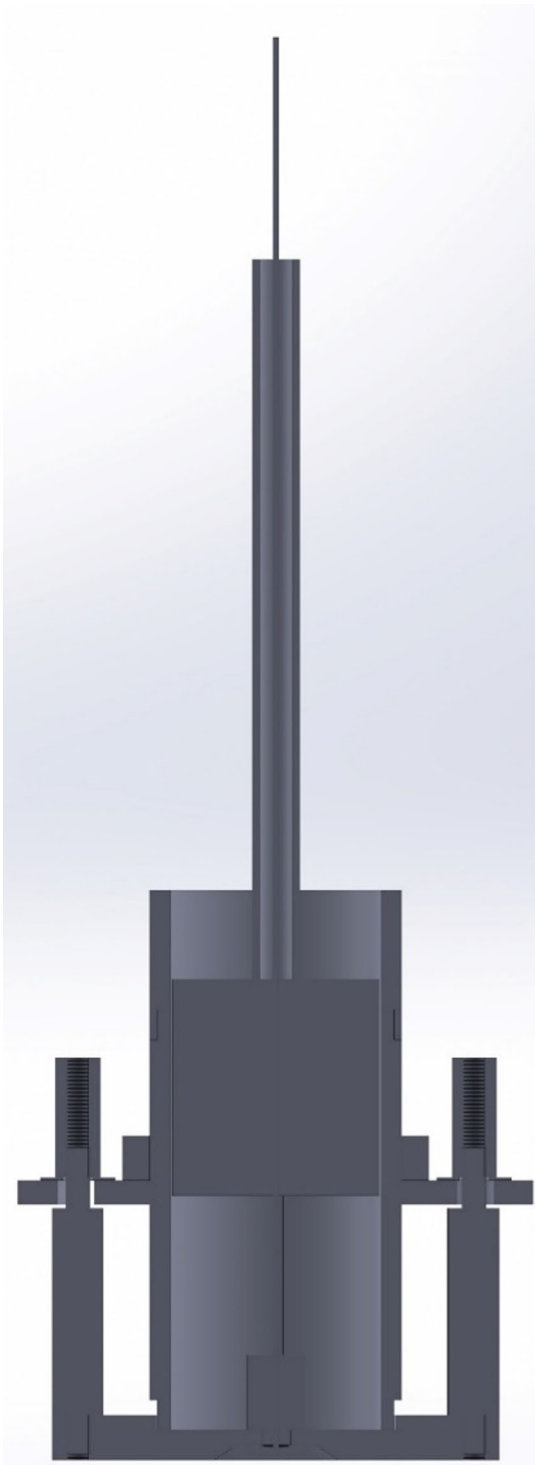

Fig. 13 Cross section of the mold, rammer, and needle

for these soil samples. The energy gradients (i) of AF1 and AF2 soil samples, calculated from the average values of the flow rates obtained for the initial hole diameter, were 6.73 and 6.91, respectively. These energy gradients decreased as the hole diameter widened by erosion. The water was collected without water pressure control. This may cause the energy gradient to not be under control [54]. Although there is no water pressure control in the test equipment, the energy gradient of the flow can be calculated with the help of hydraulic models based on the developed pipe hydraulics theorem. Moreover, Reynolds numbers can be calculated, and the flow regime (laminar/turbulent) can be controlled. In the tests performed on AF1 and AF2 soil samples, the lowest Reynolds numbers were determined as 3420 and 3825 with 2-mm hole diameter and 4612 and 5360 with 4-mm hole diameter, respectively. According to the Reynolds numbers, the flow is turbulent in the tests.

Table 9 Measured and target water contents and saturation degrees of soil samples

Sample Name	Sample Code	w_{tar}(%)	w_{mea} (%)	Δ (%)	S_r (%)
Afyon-1	AF1_1IL	24.3	24.5	0.82	88.3
	AF1_2WL		24.6	1.23	88.7
	AF1_3WL		24.6	1.23	88.7
	AF1_4WL		24.7	1.65	89.0
Afyon-2	AF2_1IL	22.1	23.2	4.98	81.5
	AF2_2WL		23.7	7.24	83.2
	AF2_3WL		23.9	8.14	83.9
	AF2_4WL		23.6	6.79	82.9
Çatören dam	ÇAT_1IL	20.0	19.9	− 0.50	89.0
	ÇAT_1C		19.7	− 1.50	88.1
	ÇAT_2WL		19.5	− 2.50	87.2
	ÇAT_3WL		20.1	0.50	89.8
	ÇAT_4WL		19.6	− 2.00	87.6
Kunduzlar dam	KUN_1IL	23.5	23.4	− 0.43	84.6
	KUN_2WL		24.1	2.55	87.1
	KUN_3WL		24.1	2.55	87.1
	KUN_4WL		23.5	0.00	84.9

The variation of the erosion rates of the AF1 and AF2 dispersive soil samples, which were dependent on the average principal stress ratios, is shown in Fig. 16. The concentrated leak erosion resistance and erosion behavior of these dispersive soil samples employed in the current study were investigated in the test equipment developed and used in the present study for stress-free conditions [56], published previously. The erosion rates calculated in the AF1 and AF2 soil samples in stress-free conditions were 10.21 and 5.05 kg/m^2/s, respectively, while t_2 (the time-critical shear stresses were compared) was 30 and 90 s, respectively. According to Fig. 16 and the erosion rate values mentioned above, the erosion rates in the soil samples decreased under given stress conditions. The principal stress ratios in the initial hole diameters were considered for the critical shear stresses using t_2 (Fig. 17).

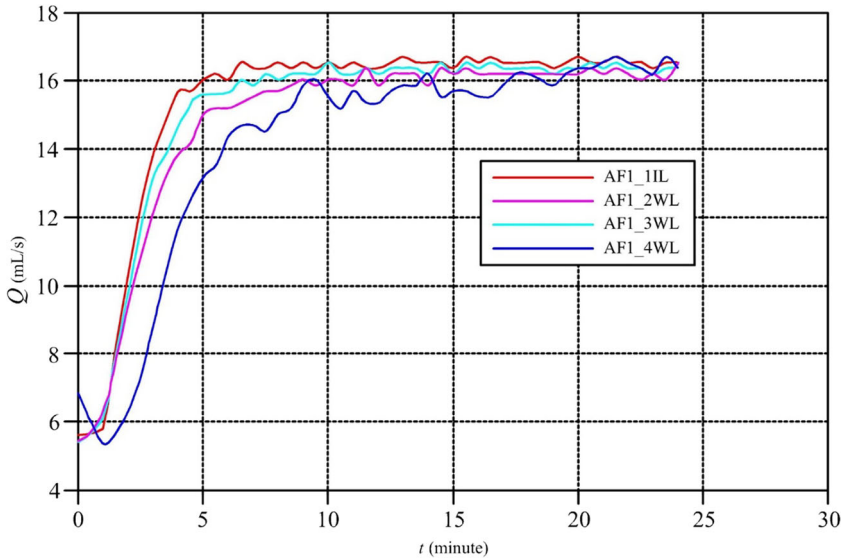

Fig. 14 Time-dependent flow rate changes under different loading conditions for the AF1 soil sample

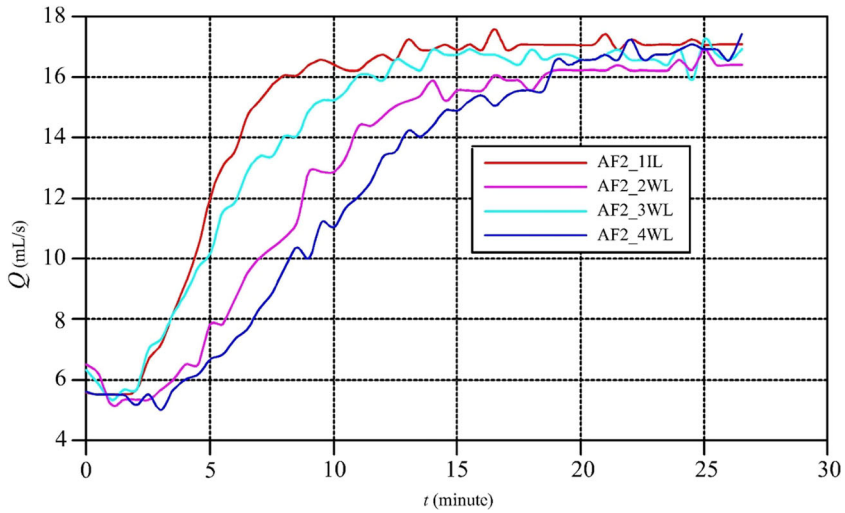

Fig. 15 Time-dependent flow rate changes under different loading conditions for the AF2 soil sample

Dispersive erosion is controlled by clay in dispersive soils. The sand/clay ratios of the AF1 and AF2 soil samples were 0.45 and 2.11, respectively. The reason for using the sand/clay ratio rather than the clay ratio is that the erosion resistance of sand varies depending on the average grain size, unlike fine-grained soils [9]. Furthermore, silts are more susceptible to erosion than clays in dispersive soils [15]. According to Fig. 17, in the AF1 soil sample with a lower sand/clay ratio, the stress conditions did not significantly affect its critical shear stresses. In both samples, there was no significant relationship between the middle principal stresses (σ_{2h}) and erosion rate or critical shear stresses (see Fig. 16 and Fig. 17). According to Figs. 16 and 17, the stresses affecting erosion rate and critical shear stresses were determined to be the maximum (σ_{1h}) and minimum (σ_{3h}) principal stresses. As the σ_{1h}/σ_{3h} ratio increased, the erosion rate increased in both samples. Only in the AF2 soil sample, which had a higher sand/clay ratio, did the critical shear stresses decrease as the σ_{1h}/σ_{3h} ratio increased. There is no meaningful effect of stress conditions on critical shear stresses in the AF1 soil sample.

Besides, in the soil samples with similar clay mineralogy, defined as the same dispersive category according to physical and chemical tests, the erosion rates in the AF1 soil sample with a lower sand/clay ratio were higher for all loading conditions than the AF2 soil. In contrast, the critical shear stresses in the AF1 soil sample were lower. In other words, the erosion resistance of the AF1 soil sample is less than that of the AF2 soil sample.

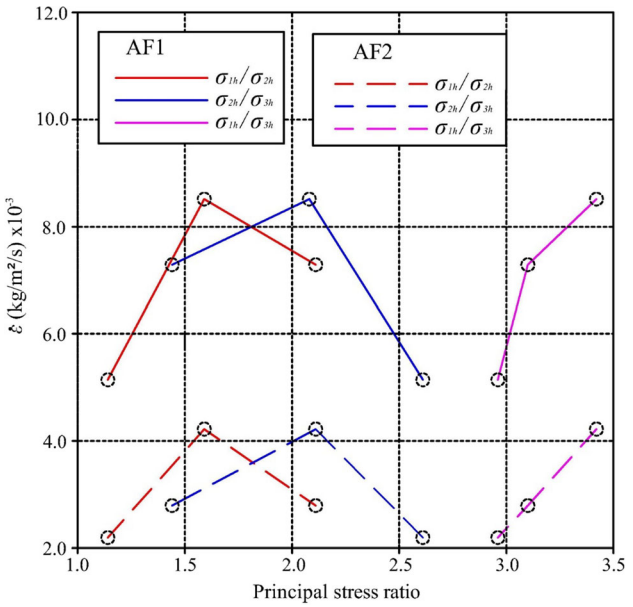

Fig. 16 Variation of erosion rates with respect to the principal stress ratio in dispersive soil samples

For stressed conditions in dispersive soil samples that have a larger sand/clay ratio, the internal erosion resistance shows a behavior similar to the failure strength in the Mohr–Coulomb hypothesis. It is assumed in the Mohr–Coulomb hypothesis that the middle principal stresses do not affect the failure of soils [31]. Similarly, in this study, the middle principal stresses (σ_{2h}) developed in the hole wall did not affect internal erosion resistance. As the σ_{1h}/σ_{3h} ratio increases, the shear stresses in the hole wall plane also increase; accordingly, the stress conditions in the hole wall plane approach the failure behavior of the Mohr–Coulomb hypothesis. As a result, internal erosion resistance decreases.

When examining the holes of the AF1_1IL and AF2_1IL samples (which were photographed and enlarged after the experiment), it was observed that backward erosion occurred near the point where flow exited the hole in the AF2_1IL sample, which had a higher sand/clay ratio (Fig. 18). In addition, in the AF1_1IL sample, internal erosion occurred as concentrated leak erosion [56].

As shown in Fig. 19, the AF1 soil sample shows similar internal erosion behavior in the stressed condition compared to the stress-free condition shown above. In the AF2 soil sample, the backward erosion at the point where flow exited the hole decreased considerably due to applied stresses (see Fig. 20).

The time-dependent flow rate curves of the KUN non-dispersive soil sample under different loading conditions are given in Fig. 21.

The flow rates measured at the initial hole diameter, the average energy gradient, the Reynolds numbers, and the measured cumulative water volumes under different loading conditions for the KUN soil sample are shown in Table 10. As shown in Fig. 21 and Table 10, in the non-dispersive KUN sample, the stresses applied to the samples did not affect their erosion resistance. However, negligible hole recovery was observed in the KUN_3WL and KUN_4WL samples. Due to the applied stresses, the cumulative volume of water passing through the hole slightly decreased compared to the stress-free condition.

The time-dependent flow rate curves for the ÇAT sample, which was determined to be the intermediate soil in the pinhole test and by using TDS-Na(%) and CEC-

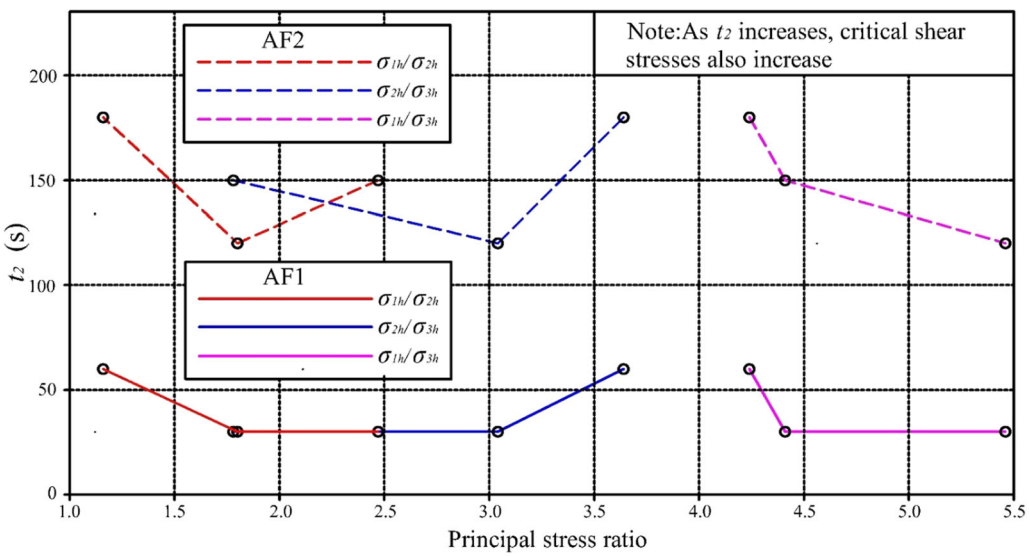

Fig. 17 Variation of critical shear stresses with respect to the principal stress ratio in dispersive soil samples

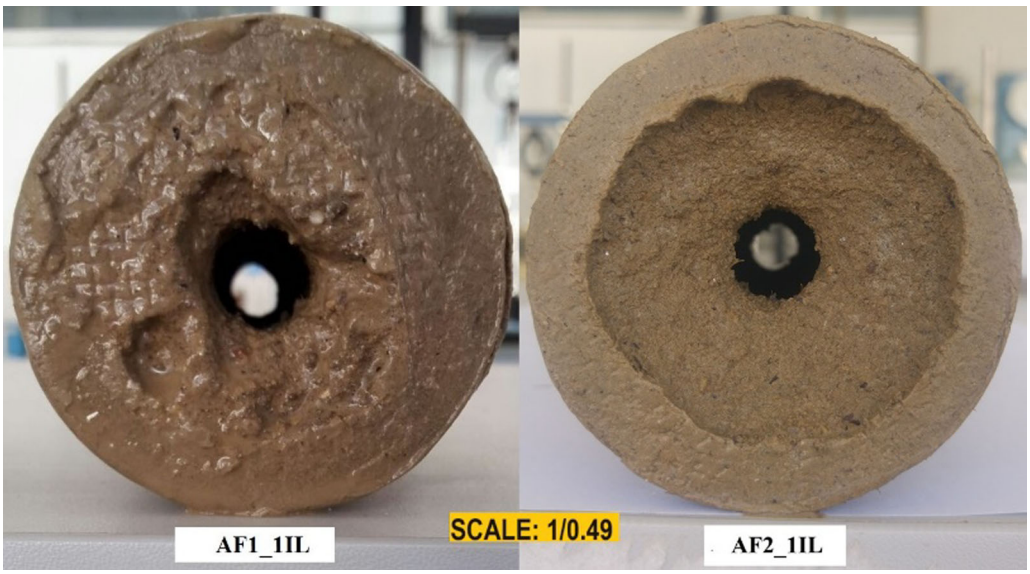

Fig. 18 Post-experimental images of the AF1_1IL and AF2_1IL soil samples (Retrieved from [56])

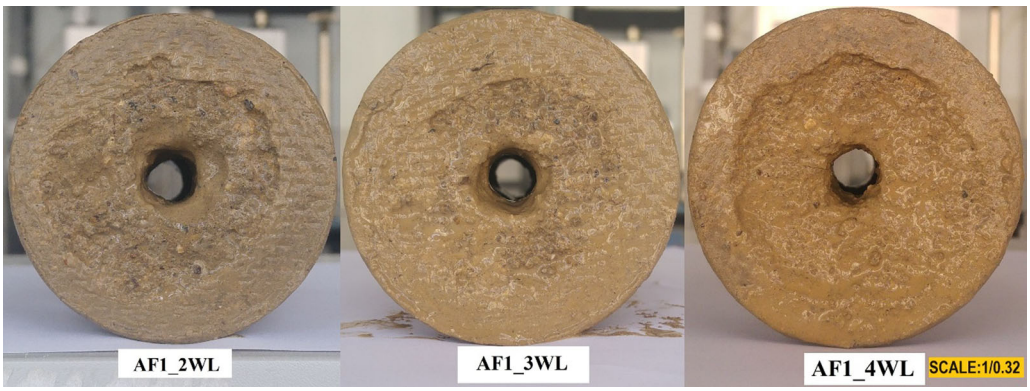

Fig. 19 Post-experimental images of the AF1 soil sample after different loading conditions

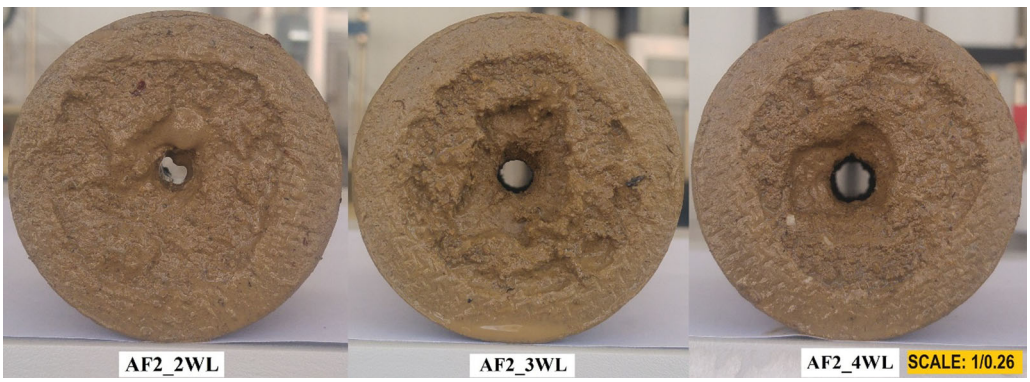

Fig. 20 Post-experimental images of the AF2 soil sample after different loading conditions

ESP(%)under different loading conditions, are given in Fig. 22.

The flow rates measured at the initial hole diameter, the average energy gradient, the Reynolds numbers, and the measured cumulative water volumes under different loading conditions for the ÇAT soil sample are shown in Table 11.

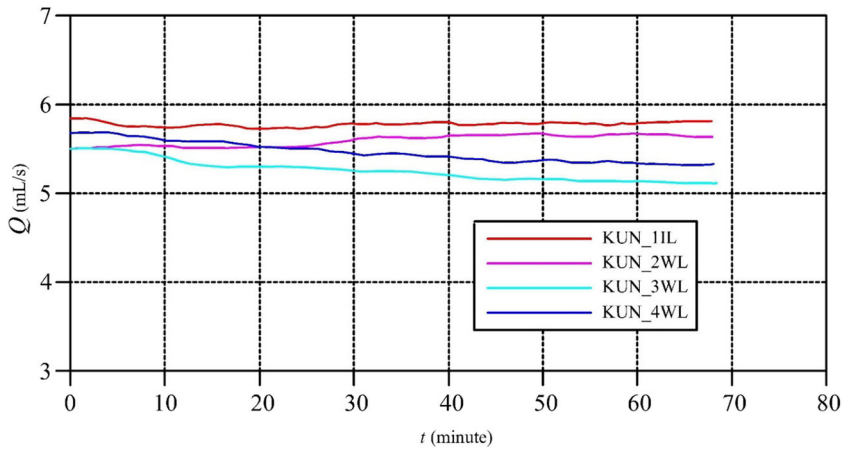

Fig. 21 Time-dependent flow rate curves of the KUN soil sample under different loading conditions

Table 10 Flow rates, average energy gradient, Reynolds numbers, and cumulative water volumes for the KUN sample

Sample Code	Q_2 (mL/s)	Q_{2ave} (mL/s)	$\Sigma\Delta h$ (m)	k_s (mm)	$\Delta h_{friction}$ (m)	i	Re	ΣV (L)
KUN_1IL	5.85	5.64	1.0871	0.11339	0.76366	6.64	3903	20.89
KUN_2WL	5.51						3676	20.03
KUN_3WL	5.51						3676	19.84
KUN_4WL	5.68						3789	20.11

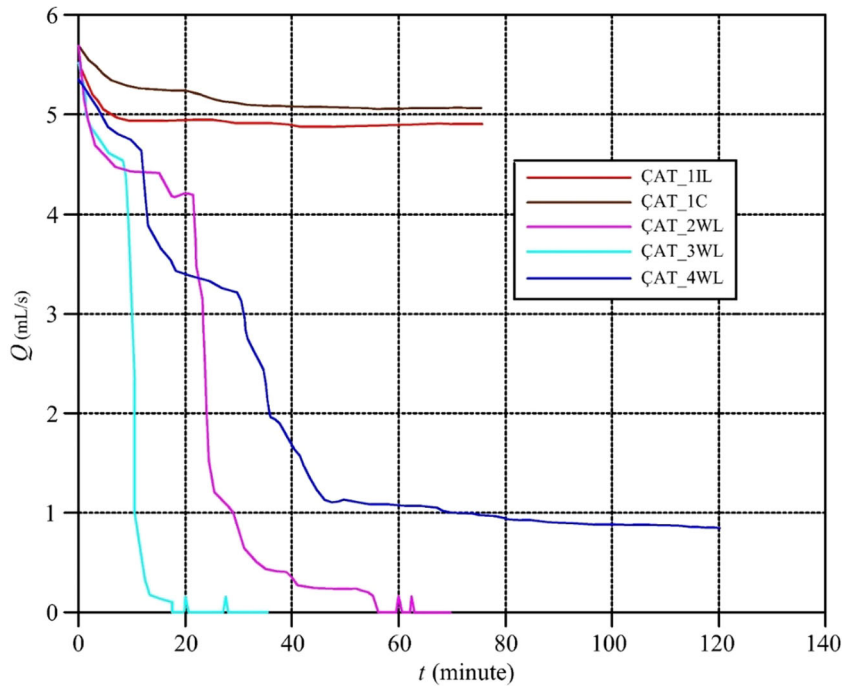

Fig. 22 Time-dependent flow rate changes in the ÇAT soil sample under different loading conditions

As shown in Fig. 22 and Table 11, the soil on the hole wall in the ÇAT sample (which consisted of intermediate soil and vermiculite clay mineral) recovered by swelling radially under the given loading conditions. As the recovery time of the hole in soil samples increases, the swelling ratio of the soil in the hole wall decreases. Swelling ratios of fine-grained soils decrease with increasing pre-swelling water contents, but they increase as

Table 11 Flow rates, average energy gradient, Reynolds numbers, and cumulative water volumes for the ÇAT sample

Sample code	Q_2 (mL/s)	Q_{2ave} (mL/s)	$\Sigma\Delta h$ (m)	k_s (mm)	$\Delta h_{friction}$ (m)	i	Re	ΣV (L)
ÇAT_1IL	5.51	5.55	1.0872	0.12550	0.77283	6.72	3789	22.49
ÇAT_1C	5.68						3906	23.00
ÇAT_2WL	5.68						3906	7.10
ÇAT_3WL	5.51						3789	2.95
ÇAT_4WL	5.35						3679	13.27

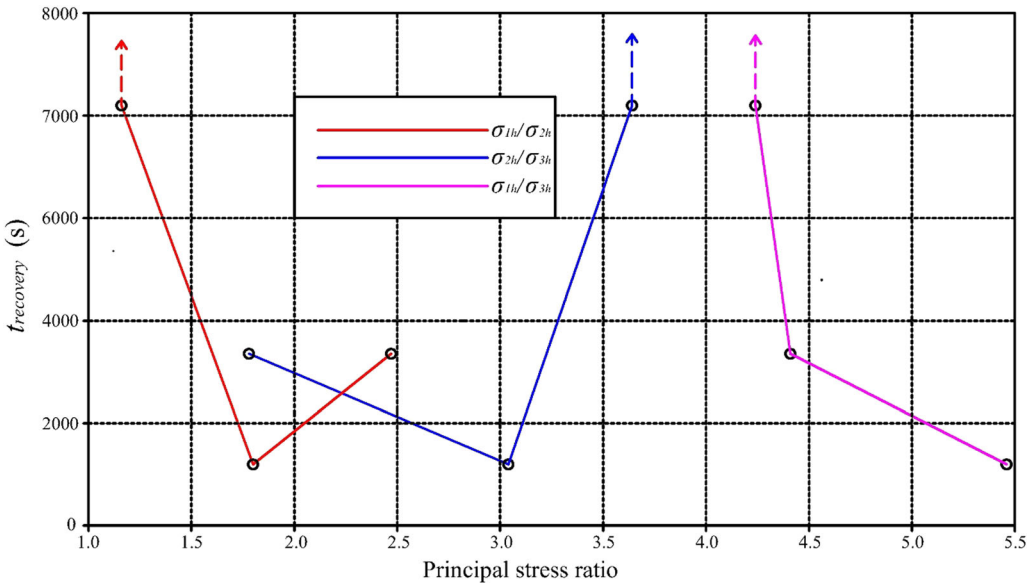

Fig. 23 Variation of the recovery time of the hole with an average principal stress ratio

their dry densities increase [26]. Due to stresses acting on soils, the spaces between grains become smaller, and their dry densities increase. With increased dry densities, repulsive forces increase between the grains, thus increasing swelling [37, 63]. Similar to those described above, the swelling ratios of the stress-acted ÇAT_2WL, ÇAT_3WL, and ÇAT_4WL samples were higher than those of ÇAT_1IL and ÇAT_1C samples when tested in stress-free conditions. The holes in ÇAT_2WL and ÇAT_3WL soil samples were blocked at approximately 60th and 20th minutes due to the swelling effect and stopped the water flow, respectively.

Again, according to Fig. 22, in the ÇAT_1IL and ÇAT_1C samples, slight recovery was seen in the hole, but then the flow rates passing through the hole became constant. Higher flow rates were obtained in the ÇAT_1C sample compared to the ÇAT_1IL sample. In the ÇAT_1C sample, which was kept in the curing environment for 24 h, the soil swelled slightly, and the hydraulic roughness decreased due to the stressed surface on the hole wall, thus allowing much more flow to pass through the hole. On the other hand, keeping soil samples in the curing environment for 24 h did not affect the recovery of the hole.

Moreover, the recovery time of the hole in the ÇAT soil sample was controlled by maximum and minimum principal stresses. As the σ_{1h}/σ_{3h} ratio decreased, the recovery time of the hole increased, and swelling ratios decreased (Fig. 23).

4 Conclusion

This study investigated the effects of stress conditions on the concentrated leak erosion resistance of dispersive, intermediate, and non-dispersive cohesive soil samples under a single hydraulic head. While phengite is the dominant clay mineral in two different dispersive soil samples, vermiculite is the dominant clay mineral in the intermediate soil sample. However, palygorskite is the dominant clay mineral in the non-dispersive soil sample. In the tests performed under four different loading conditions, such as stress-free, anisotropic-expansion, isotropic, and anisotropic-compression, the stresses developed in the hole

wall were determined by numerical modeling as pre-experimental stress conditions.

According to the results of the experiments performed on dispersive soil samples with similar clay mineralogy and erosion sensitivity, the stress conditions significantly affect the erosion rate and the critical shear stress in the soil sample with a larger sand/clay ratio with dispersive erosion. This effect is only valid for the erosion rate in the soil sample with a smaller sand/clay ratio. Furthermore, the failure of the dispersive erosion resistance of fine-grained soils can be explained by the shear failure phenomenon in the Mohr–Coulomb hypothesis in the dispersive soil sample with a larger sand/clay ratio. When the shear stresses in a hole wall are higher (as the σ_{1h}/σ_{3h} ratio increases), critical shear stresses cause internal erosion to decrease and erosion rates to increase. However, while concentrated leak erosion was observed in the soil sample with a smaller sand/clay ratio, it was detected that backward erosion developed along with concentrated leak erosion in the soil sample with a larger sand/clay ratio. The backward erosion decreases under stressed conditions.

No concentrated leak erosion was observed in the non-dispersive soil sample in the stressed and unstressed conditions at the hydraulic head considered during the tests. Therefore, the effect of stress conditions on the non-dispersive soil sample could not be seen. The amount of recovery observed in the stress-free condition in intermediate soil samples with vermiculite clay mineral increased with the effect of stressed conditions. The amount of recovery increased as the σ_{1h}/σ_{3h} ratio in the hole wall increased.

Acknowledgements This manuscript has been extracted from a PhD dissertation conducted at Eskişehir Osmangazi University. All data, models, and code generated or used during the study appear in the published article

Funding Open access funding provided by the Scientific and Technological Research Council of Türkiye (TÜBİTAK).

Data availability The data that support the findings of this study are available from the corresponding author, upon reasonable request.

Declarations

Conflict of interest The authors declare no conflict of interest.

References

1. Aitchison GD, Wood CC (1965) Some interactions of compaction, permeability and post-construction deflocculation affecting the probability of piping failure in small earth dams (expanded version of this paper constitutes the CP 029). In: Proceedings of the 6th ınternational conference on soil mechanics and foundation engineering, toronto, Canada, pp 442–446
2. Alizadeh A (1974) Amount and type of clay and pore fluid influences on the critical shear stress and swelling of cohesive soils. Ph. D. Dissertation, University of California
3. Arulanandan K, Sargunam A, Loganathan P, Krone RB (1973) Application of chemical and electrical parameters to prediction of erodibility. In soil erosion: causes and Mechanisms; prevention and Control. Highw Res Board Spec Rep 135:42–51
4. Attom M (2012) The effect of compaction and initial water content on soil erosion. In: The international conference on scour and erosion, Paris, p 27–31
5. Benahmed N, Bonelli S (2012) Investigating concentrated leak erosion behaviour of cohesive soils by performing hole erosion tests. Eur J Environ Civ Eng 16(1):43–58. https://doi.org/10.1080/19648189.2012.667667
6. Bhasin RN, Lovell CW, Jr Foebes GH (1969) Erodability of sand-clay mixtures as evaluated by a water jet. Water Resources Research Center, Purdue University, Lafayette, Ind., Technical Report No. 8
7. Bonelli S (2013) Erosion in geomechanics applied to dams and levees. Hoboken, USA
8. Brandenburg K, Putz H (2006) Diamond. Crystal Impact GbR, Bonn Germany
9. Briaud JL, Ting FCK, ChenR HC et al (1999) SRICOS: prediction of scour rate in cohesive soils at bridge piers. J Geotechnical Geoenviron Eng 125(4):237–246. https://doi.org/10.1061/(ASCE)1090-0241(1999)125:4(237)
10. Briaud JL (2001) Introduction to soil moduli. Geotechnical News 19(2):54–58
11. Budhu M (2010) Soil Mechanics and Foundation–3rd Edition. Arizona, USA
12. Burns B, Ghataora GS (2007) Internal erosion of kaolin. In Problematic Soils Rocks In Situ Characterization. https://doi.org/10.1061/40906(225)6
13. Cedeno ARJ (1998) Piping in Dams: Tests to asses the factors which affect progression. Project/Thesis, School of Civil and Enviromental Engineering, University of New South Wales, CIVL4906.
14. Christensen RW, Das BM (1973) Hydraulic erosion of remolded cohesive soils. In soil erosion: causes and mechanism; prevention and control. Highway Res Board Special Report 135:8–19
15. Curtin D, Steppuhn H, Selles F (1994) Clay dispersion in relation to sodicity, electrolyte concentration, and mechanical effects. Soil Sci Soc Am J 58(3):955–962. https://doi.org/10.2136/sssaj1994.03615995005800030045x
16. Decker RS, Dunnigan LP (1977) Development and use of the soil conservation service dispersion test. In: Sherard J, Decker R (eds) in STP623-EB dispersive clays, related piping, and erosion in geotechnical projects. West Conshohocken, PA, ASTM International, pp 94–109
17. Dunn IS (1959) Tractive resistance of cohesive channels, journal of soil mechanics and foundations division. Am Soc Civil Eng 85(SM3):1–214. https://doi.org/10.1061/JSFEAQ.0000195

18. Emerson WW (1967) A Classification of soil aggregates based on their coherence in water. Aust J Soil Res 5:47–57. https://doi.org/10.1071/SR9670047
19. Farzin MH, Krizek RJ, Corotis RB (1975) Evaluation of modulus and poisson's ratio from triaxial tests. Transp Res Rec 537:69–80
20. Fell R, Foster M, Davidson R et al (2008) A unified method for estimating probabilities of failure of embankment dams by internal erosion and piping. UNICIV Report R 446:10–18
21. Foster M, Fell R, Spannagle M (2000) The statistics of embankment dam failures and accidents. Can Geotech J 37(5):1000–1024. https://doi.org/10.1139/t00-030
22. Gerber FA, Harmse VM (1987) Proposed procedure for identification of dispersive soils by chemical testing. Civil Engineer South Africa 29(10):397–399
23. Ghebreiyessus YT, Gantzer CJ, Alberts EE, Lentz RW (1994) Soil erosion by concentrated flow, shear stress and bulk density. Transactions ASAE 37(6):1791–1797. https://doi.org/10.13031/2013.28268
24. Haghighi I, Chevalier C, Duc M, Guédon S, Reiffsteck P (2013) Improvement of hole erosion test and results on reference soils. J Geotechnical Geoenviron Eng 139(2):330–339. https://doi.org/10.1061/(ASCE)GT.1943-5606.0000747
25. Hjeldness EI, Lavania BV (1980) Cracking, leakage, and erosion of earth dam materials. J Geotechnical Geoenviron Eng 106(ASCE 15220). https://doi.org/10.1061/AJGEB6.0000917
26. Holtz WG, Gibbs HJ (1956) Engineering properties of expansive clays. Trans ASCE 121:641–677. https://doi.org/10.1061/TACEAT.0007325
27 . ICOLD C (2012) Internal erosion of existing dams, levees and dikes, and their foundations, Draft Bulletin International Commission on Large Dams, Paris, 164
28. Kandlikar SG (2006) Single-phase liquid flow in minichannels and microchannels. Heat Transfer And Fluid Flow in Minichannels And Microchannels, 2nd edn. Elsevier, Amsterdam, pp 103–174
29. Koltuk S, Azzam R (2019) Use of quicksand condition to assess the base stabilities of sheeted excavation pits against seepage failure in cohesionless soils. Arab J Sci Eng 44(10):8515–8526. https://doi.org/10.1007/s13369-019-03890-y
30. Khodaparast M, Rajabi AM, Moein B, Bazargan J (2021) Identifying dispersive soils by modification of chemical criterion, validated based on data from Northwest and Central Iran. Arab J Geosci 14(17):1–11. https://doi.org/10.1007/s12517-021-08130-y
31. Labuz JF, Zang A (2012) Mohr–Coulomb Failure Criterion. Rock Mech Rock Eng 45:975–979. https://doi.org/10.1007/s00603-012-0281-7
32. Lewis D, Schmidt N (1977) Erosion of unsaturated clay in a Pinhole Test. In: Sherard J, Decker R (eds) Dispersive Clays, Related Piping, and Erosion in Geotechnical Projects. ASTM International, West Conshohocken PA, pp 260–273
33. Liou YD (1970) Hydraulic erodibility of two pure clay systems. Ph. D. Dissertation, Colorado State University, Fort Collins, Colorado
34. Lyle WM (1964) The effect of void ratio on critical tractive force of cohesive soils. M. S. Dissertation, Texas A&M University, College Station, Texas
35. Lyle WM, Smerdon ET (1965) Relation of compaction and other soil properties to erosion resistance of soils. Transactions American Soc Agric Engineers 10(13031/2013):40536
36. Meeuwig RO (1971) Soil stability on high-elevation rangeland in the ıntermountain area. Research Paper, U. S. Department of Agriculture Forest Service, Intermountain Forest and Range Experiment Station, Ogden, Utah, INT-94.
37. Nelson J, Miller DJ (1992) Expansive soils: problems and practice in foundation and pavement engineering. Wiley
38. Oh WT, Vanapalli SK (2011) Relationship between Poisson's ratio and soil suction for unsaturated soils. In: Proc., 5th Asia-Pacific Conf. on Unsaturated Soils Bangkok, Kasetsart University, Thailand, pp 239–245
39. Ozen M (2012) Mesh metric spectrum quality. California J Phys Fluid 48:236–267
40. Pahlevi MR, Munirwansyah M (2022) Assessing slope failure of soil erodibility problem by soil dispersive identification, In: E3S Web of Conferences, 340: 01006
41. Paige-Green P (2008) Dispersive and erodible soils–Fundamental differences. In: SAIEG/ SAICE Problem Soils Conference, Midrand, pp 59–67
42. Petry TM (1974) Identification of dispersive clay soils by a physical test. Ph. D. Dissertation, Oklahoma State University, Stillwater, Oklahoma
43. Regazzoni PL, Marot D (2011) Investigation of interface erosion rate by Jet erosion test and statistical analysis. Eur J Environ Civ Eng 15(8):1167–1185. https://doi.org/10.1080/19648189.2011.9714847
44. Richards LA (1954) Methods for Soil Characterization. In Diagnosis and Improvement of Saline and Alkali Soils. U.S. Department of Agriculture, Washington DC
45. San Lim S (2006) Experimental investigation of erosion in variably saturated clay soils, Ph.D. thesis, University of New South Wales.
46. San Lim S, Khalili N (2009) An improved rotating cylinder test design for laboratory measurement of erosion in clayey soils. Geotech Test J 32(3):1–7. https://doi.org/10.1520/GTJ101448
47. Sargunan A (1977) Concept of critical shear stress in relation to characterization of dispersive clays. In: Sherard J, Decker R (eds) Dispersive Clays, Related Piping, and Erosion in Geotechnical Projects. ASTM International, West Conshohocken PA, pp 390–397
48. Shaikh A, Ruff JF, Abt SR (1988) Erosion rate of compacted Na-montmorillonite soils. J Geotechnical Eng 114(3):296–305. https://doi.org/10.1061/(ASCE)0733-9410(1988)114:3(296)
49. Shaikh A, Ruff JF, Charlie WA, Abt SR (1988) Erosion rate of dispersive and nondispersive clays. J Geotechnical Eng 114(5):589–600. https://doi.org/10.1061/(ASCE)0733-9410(1988)114:5(589)
50. Sherard JL, Decker RS, Ryker NL (1972) Piping in earth dams of dispersive clay In performance of earth and earth-supported structures. American Society of Civil Engineers, New York, p 589
51. Sherard JL, Dunnigan LP, Decker RS (1976) Identification and nature of dispersive soils. J Geotech Eng Div 102(GT4):298–312
52. Sherard JL, Steele EF, Decker RS, Dunnigan LP (1976) Pinhole test for identifying dispersive soils. J Geotech Eng Div 102(1):69–85. https://doi.org/10.1061/AJGEB6.0000236
53. Singh VP (1996) Dam Breach Modelling Technology Water Science and Technology Library. Kluwer Academic Publishers, Dordrecht, Boston, London, p 17
54. To P, Price P (2021) Influence of rate of hydraulic gradient on washed-out soil mass due to perpendicular contact erosion or poor filter design. In: Proceedings of the 10th International Conference on Scour and Erosion, Online, pp 50–58
55. Topçu S (2020) Comparative analysis of internal erosion behaviour for fine grained soils under different stress state. Doctoral Dissertation, Department of Civil Engineering, Eskişehir Osmangazi University.
56. Topçu S, Tosun H (2021) Determination of dispersive erosion resistance in fine-grained soils with newly developed test equipment. Geotechnical Testing J. https://doi.org/10.1520/GTJ20200213

57 . U.S. Bureau of Reclamation (1990) Earth Manual Part 2. 3rd ed. Denver, CO: Materials engineering branch Research Laboratory Services Division
58. U.S. Bureau of Reclamation (1990) Determining dispersibility of clayey soils by the crumb test method, USBR 5400. U.S. Bureau of Reclamation, Denver, CO
59. U.S. Bureau of Reclamation (1990) Determining dispersibility of clayey soils by the double hydrometer test method, USBR 5405. U.S. Bureau of Reclamation, Denver, CO
60. U.S. Bureau of Reclamation (1990) Determining dispersibility of clayey soils by the pinhole test method, USBR 5410. U.S. Bureau of Reclamation, Denver, CO
61. U.S. Bureau of Reclamation (2015) Internal Erosion Risks for Embankments and Foundations. Technical Report IV-4, Denver, CO: U.S. Bureau of Reclamation
62 Velde BB, Meunier A (2008) The origin of clay minerals in soils and weathered rocks, Springer, Berlin
63. Villar MV, Lloret A (2008) Influence of dry density and water content on the swelling of a compacted bentonite. Appl Clay Sci 39(1–2):38–49. https://doi.org/10.1016/j.clay.2007.04.007
64. Wahl TL (2010) Relating HET and JET test results to internal erosion field tests. In: Joint federal interagency conference on sedimentation and hydrologic modeling.
65. Wan CF, Fell R (2002) Investigation of internal erosion and piping of soils in embankment dams by the soil slot erosion test and the hole erosion test. UNICIV Report No. R-412. New South Wales, Australia: University of New South Wales, School of civil and environmental engineering.
66. Yunus AC (2010) Fluid Mechanics: Fundamentals and Applications (Si Units). Delhi, India
67. Yüksel Y (2012) Fluids Mechanics and Hydraulic. İstanbul, Turkey
68. Zhang LM, Xu Y, Jia JS (2009) Analysis of earth dam failures: a database approach. Georisk 3(3):184–189. https://doi.org/10.1080/17499510902831759